Flow Pattern and Heat Transfer in Tube Banks of a Simulated Fluidized-Bed Heat Exchanger*

Mamoru OZAWA**, Hisashi UMEKAWA**,
Takeshi MATSUDA**, Nobuyuki TAKENAKA***
and Masahito MATSUBAYASHI****

A simulated fluidized-bed heat exchanger with tube banks was visualized using a neutron radiography system. Observed flow pattern indicated an importance of the tube arrangement. Heat transfer experiment, conducted simultaneously, indicated a close relationship between the heat transfer and flow pattern. The staggered arrangement with relatively small pitch has a potential of high heat transfer performance.

Key Words: Fluidized Bed, Heat Transfer, Heat Exchanger, Multi-phase Flow, Flow Visualization, Digital Image Processing

1. Introduction

Heat transfer characteristics of tubes immersed in a fluidized-bed have been widely investigated so far, and the principal heat transfer mechanism has been classified into three categories, i.e. solid convection, gas convection and radiation. The extensive and critical reviews were presented by Horio[1] and Saxena et al.[2),(3)] with regard to convective heat transfer including solid and gas convections. Saxena et al.[2),(3)] discussed the heat transfer characteristics in tube banks, and emphasized a great importance of the tube arrangement.

As is clearly observed in their discussions, many empirical constants are included in heat transfer correlations. In order to determine these constants reasonably, Kurosaki et al.[4] and Miyamoto et al.[5),(6)] investigated particle behavior on and near the heat transfer surface using optical fiber probes. Alternative approach discussed in this report is based on the concept that the flow pattern in tube banks plays an important role in the mixing process in the wake as well as the passage in the banks, similar to the case of convective heat transfer surface of boiler-superheater[7]. This approach was realized by conducting simultaneous measurement of heat transfer and the visualization of flow pattern in the banks using a neutron radiography technique.

2. Experimental Setup

The experimental setup, shown in Fig. 1, is a slender rectangular fluidized-bed model with dimensions of 300 mm width, 600 mm height and 100 mm depth. The wall material of the setup is aluminum and the bed material was sand of 99.7% SiO_2 (mean diameter: d_p=0.218 mm, density: 2 555 kg/m^3). Aeration of nitrogen gas for fluidization was conducted at the bottom through a baffle plate and a distributor plate. The distributor plate was so constructed as to form a uniform upward flow of bubble in the center part of the bed. The stagnant bed height without tube banks was set at 350 mm, and the minimum fluidization velocity was J_{Gmf}=0.058 m/s.

The tube banks are mainly composed of aluminum rods of D=40 mm O.D., and are arranged, as shown in Fig. 1, in-line with lateral pitch of H/D=1.5

* Received 13th July, 1997
** Dept. of Mechanical Engineering, Kansai University, 3-3-35 Yamate-cho, Suita, Osaka 564-8680, Japan
*** Dept. of Mechanical Engineering, Kobe University, 1-1 Rokkodai-cho, Nada-ku, Kobe 657-8501, Japan
**** Tokai Research Establishment, Japan Atomic Energy Research Institute, Tokai-mura, Ibaraki 319-1195, Japan

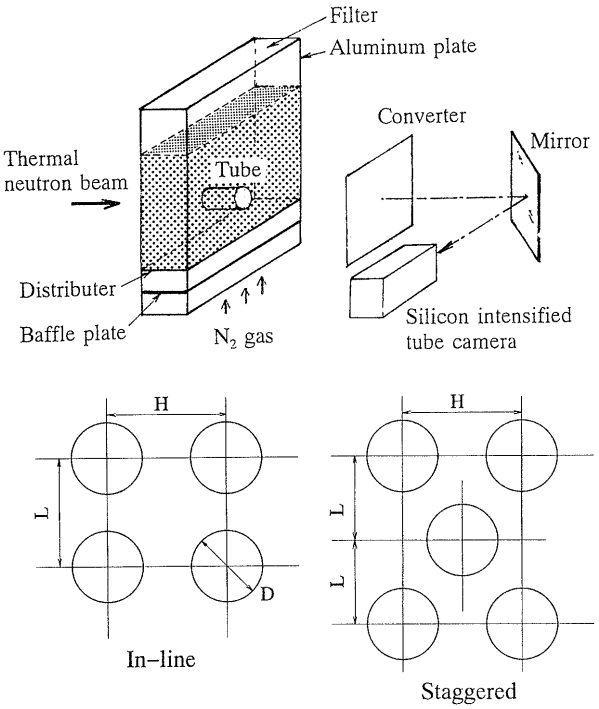

Fig. 1 Experimental setup and tube arrangement

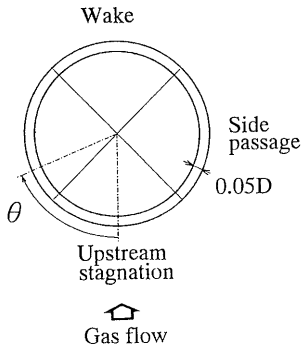

Fig. 2 Integration area around tube

and 2.0, and longitudinal pitch of $L/D=1.5$, 2.0 and 3.0; and in staggered arrangement with $H/D=1.5$ and 2.0, and $L/D=1.5$. Such tube banks were installed at 200 mm above the distributor. In the heat transfer experiments, two tubes longitudinally arranged in the banks were replaced by heat transfer tubes, in which sheathed heaters were inserted. The heat transfer tube has dimensions of 39 mm O.D. and 1 mm thickness of SUS304 steel. Twelve thermocouples of K-type are attached on the outer wall around the test tube periphery.

Flow visualization was conducted using the Neutron Radiography System of JRR-3M in JAERI. Since the sand is almost transparent against neutron, the sand coated by cadmium sulfate was mixed in the volumetric fraction of 0.3% with the bed material. Image processing technique was applied to the visualized image to obtain quantitative data of void fraction. Figure 2 represents an integration area of the void fraction to obtain area-averaged values discussed below. The fluid layer around the tube is segmented into the upstream stagnation, side passage and wake regions. Each segment has 90 deg. in angle and the thickness is set as 5% of the diameter, i.e. 2 mm in the present case. The detailed procedure of the image processing can be found elsewhere[8),(10)].

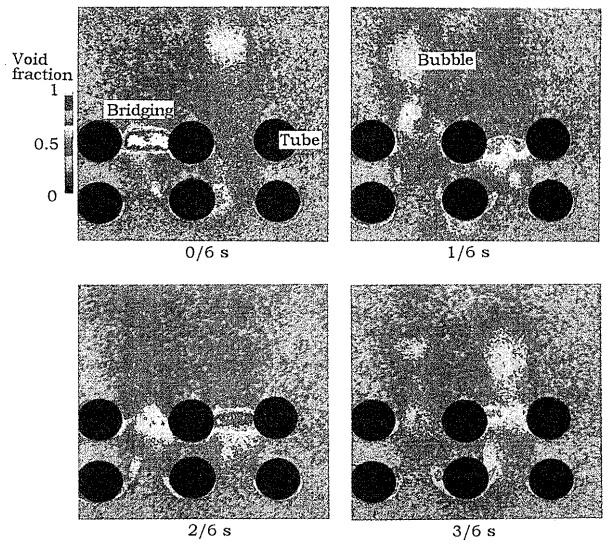

Fig. 3 Flow pattern and void fraction distribution (In-line arrangement $L/D=1.5$, $H/D=2.0$, $J_G/J_{Gmf}=1.0$)

3. Flow Pattern and Void Fraction Distribution

Figure 3 represents the processed image of void fraction distribution, obtained at $J_G/J_{Gmf}=1.0$ in the tube banks with $L/D=1.5$ and $H/D=2$ (in-line arrangement). The figure indicates clearly that the void fraction is high in the upstream stagnation region of each tube, i.e. gas pocket is formed, and that the stagnant cap of defluidized sand is formed in the wake. The stagnant cap in the wake of the 1st row is only slightly agitated by the gas flow through the side passage, owing to rather short distance between the 1st and 2nd row of the tube banks. Thus the gas pocket in the upstream stagnation region of the 2nd row is rather thin. Another typical feature is observed in the side passage of the 2nd row, i.e., a bridging is formed. This bridging continues to exist for about 0.5 to 1.5 s, expands downwards by absorbing bubbles and then collapses to form a large bubble. Such bridging was observed in the left and right passages alternatively in the present case. The bridging formation is interpreted as follows: When bubbles rise up through one passage at the 2nd row, the bed materials in the bubble wake moves upwards[11)], accordingly. The recirculation movement of the bed material may be, then, directed downwards in the neighboring region,

which results in the counter-current flow in the other passage to induce bridging formation as in a stand pipe[12),(13)]. Such feature is typical when the volumetric gas flux is relatively low.

When the volumetric gas flux is high enough as shown in Fig. 4, gas is mainly transported in the form of bubbles. The bubbles, passing through the tube banks, agitate highly the wake region as well as the side passage. Thus the bridging formation is suppressed by such intense agitation in the banks.

Successive images of 238 frames are integrated and averaged to obtain a time-averaged void fraction distribution, as shown in Fig. 5. In the arrangement of

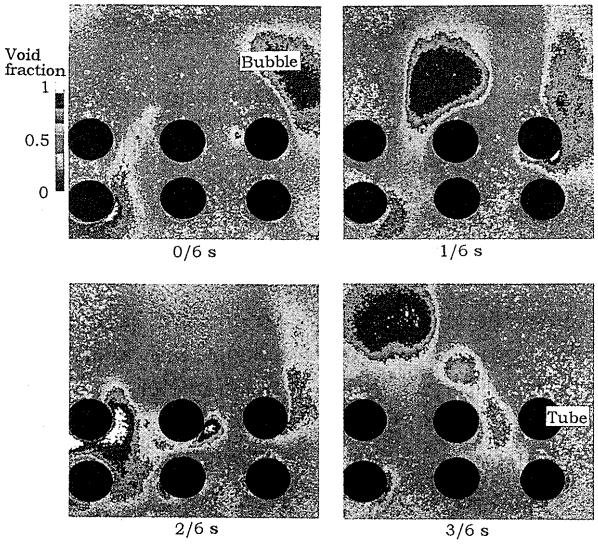

Fig. 4 Flow pattern and void fraction distribution (In-line arrangement $L/D=1.5$, $H/D=2.0$, $J_G/J_{Gmf}=4.0$)

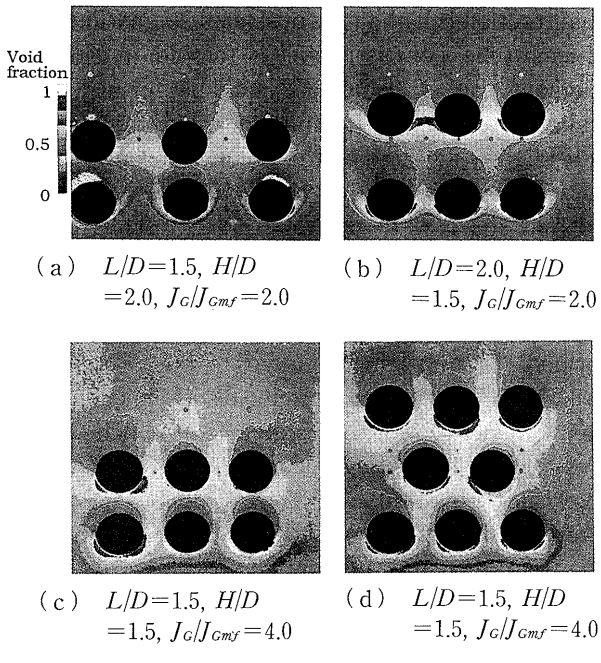

(a) $L/D=1.5$, $H/D=2.0$, $J_G/J_{Gmf}=2.0$

(b) $L/D=2.0$, $H/D=1.5$, $J_G/J_{Gmf}=2.0$

(c) $L/D=1.5$, $H/D=1.5$, $J_G/J_{Gmf}=4.0$

(d) $L/D=1.5$, $H/D=1.5$, $J_G/J_{Gmf}=4.0$

Fig. 5 Time-averaged void fraction distribution

$L/D=1.5$ and $H/D=2$, shown in Fig. 5(a), the high void fraction region is limited only in the side passages and the upstream stagnation region. In the wake region, defluidized stagnation caps with low void fraction are clearly observed. When the longitudinal pitch is relatively large and the lateral pitch is relatively small, e.g. $L/D=2$ and $H/D=1.5$, Fig. 5(b), the void fraction in the wake region of the 1st row becomes relatively high compared with the case of Fig. 5(a). This is caused by the bubble penetration into the wake region and then the agitation and/or mixing between the wake region and the bubbles through the side passage. Further increase in the gas flux in the banks with small longitudinal and lateral pitches, Fig. 5(c), bring about relatively uniform distribution of the void fraction around tube. A typical example of the void fraction distribution in the staggered arrangement is shown in Fig. 5(d) for $L/D=1.5$ and $H/D=1.5$ and $J_G/J_{Gmf}=4$. The bubbles flowing through the side passage of the 1st row are divided into two portions in the upstream stagnation region of the 2nd row tube, and then merge again around the 3rd row tube. This results in a substantial reduction in the size of the defluidized stagnation cap, which may improve the heat transfer performance owing to an intense agitation and thus solid convection.

4. Void Fraction Fluctuation

The time-varying behavior of the area-averaged void fraction for $L/D=1.5$ and $H/D=1.5$ is shown in Fig. 6. When the volumetric gas flux is low, $J_G/J_{Gmf}=1.0$, the void fractions in the upstream and wake regions indicate relatively small fluctuations at the 1st row. Especially in the wake region, the void fraction is very low, which corresponds to the defluidized stagnation cap. This is also true at the 2nd row. The void fraction in the side passage of the 1st row shows relatively small amplitude fluctuation. On the other hand, the void fraction in the side passage of the 2nd row indicates large amplitude fluctuation with rather long period. This large amplitude fluctuation is caused by the bridging in the side passage. An increase in the volumetric gas flux ($J_G/J_{Gmf}=4.0$) induces large amplitude fluctuation of void fraction in the upstream stagnation region and in the side passage as shown by dot-dash lines in Fig. 6. The formation of bridging is suppressed by the agitation of the bed materials.

5. Heat Transfer Around Tube

Heat transfer mechanisms in the fluidized-bed are gas convection, solid convection and radiation. Radiative heat transfer is so small as to be neglected

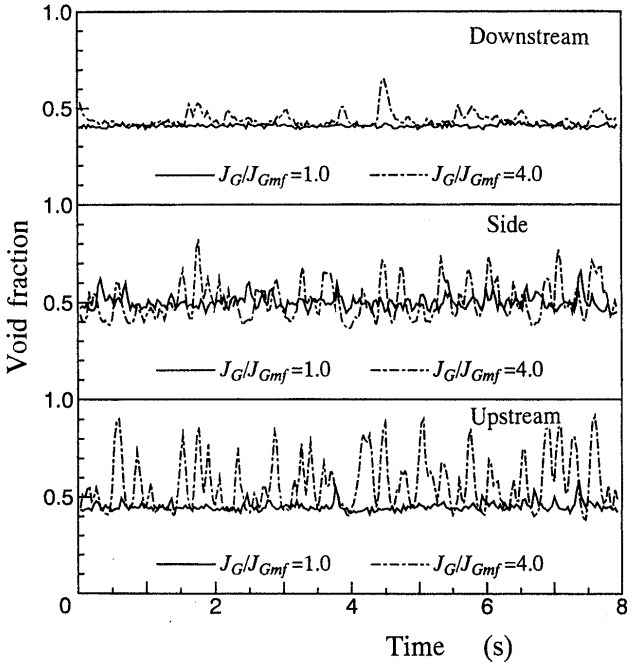

(a) 1st row

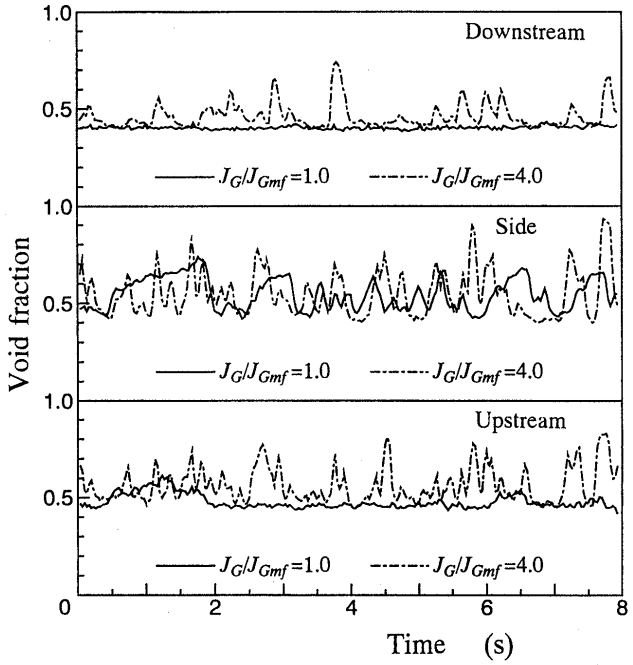

(b) 2nd row

Fig. 6 Void fraction fluctuation (In-line arrangement, L/D=1.5, H/D=1.5)

in the present experiment. The gas convection and solid convection are significantly affected by the particle movement near the heat transfer surface. As to the gas convection, the particle movement enhances turbulence in the boundary layer. The solid convection is highly dominated by the particle motion in the boundary layer as well as the mixing of solid with the surrounding region. The heat capacity of solid particle is rather large compared with the gas, and thus the

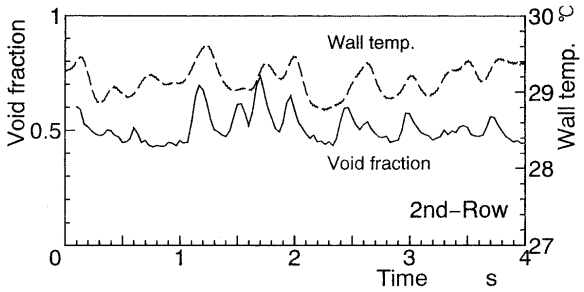

Fig. 7 Wall temperature and void fraction fluctuations (Staggered arrangement, L/D=1.5, H/D=1.5, J_G/J_{Gmf}=4.0)

heat transfer is dominated by the residence time of particle near the heat transfer surface and the time constant of heat transfer from wall-to-particle and/or gas-to-particle.

From the macroscopic point of view, the particle movement is closely related to the flow pattern and void fraction. Figure 7 demonstrates simultaneously the void fraction fluctuation in the side passage (solid line) and the wall temperature fluctuation (dashed line). The void fraction shows rather large fluctuation in the range 0.4 to 0.7, while the wall temperature fluctuates slightly with an amplitude around 0.8 K and almost synchronized with the void fraction fluctuation. When the void fraction increases, the wall temperature becomes high, but with slight time delay. This fact indicates that the heat transfer is deteriorated by an increase in the void fraction and that the solid convection is a dominant factor in the heat transfer as is pointed out by Horio[1] and Saxena et al.[2]

On the basis of the time-averaged wall and bed temperatures, the local heat transfer coefficient h around the heat transfer tube is plotted against the angle θ (see Fig. 2) from the upstream stagnation point in Figs. 8(a) to 8(d). For the in-line arrangement L/D=3 and H/D=2, Fig. 9(a), the heat transfer coefficient has maximum values at about 90 deg. and 270 deg. i.e. in the side passage. At low gas flux condition, the heat transfer coefficient is higher in the upstream stagnation region than in the wake region. An increase in the volumetric gas flux causes an increase in the heat transfer coefficient, and bring about relatively uniform distribution of heat transfer coefficient around the tube. For L/D=1.5 and H/D=2, Fig. 8(b), the general tendency is the same as the case Fig. 8(a), while the heat transfer coefficients have almost the same value in the upstream stagnation and wake regions of the 2nd row tube at low gas flux. This corresponds to the fact that the bubble penetration into the wake region is rather weak in this tube arrangement. In spite of the existence of

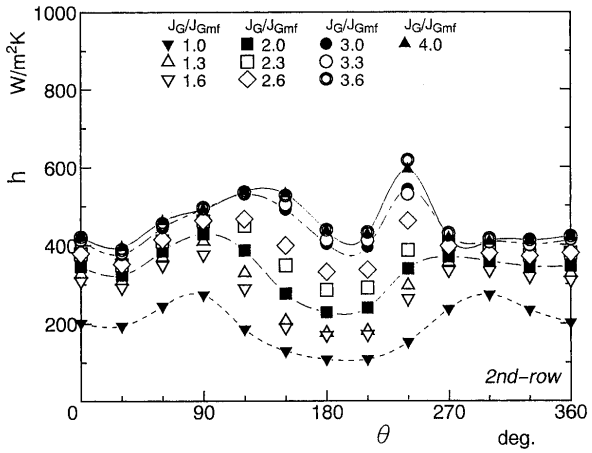

(a) In-line arrangement, $L/D=3.0$, $H/D=2.0$, 2nd row

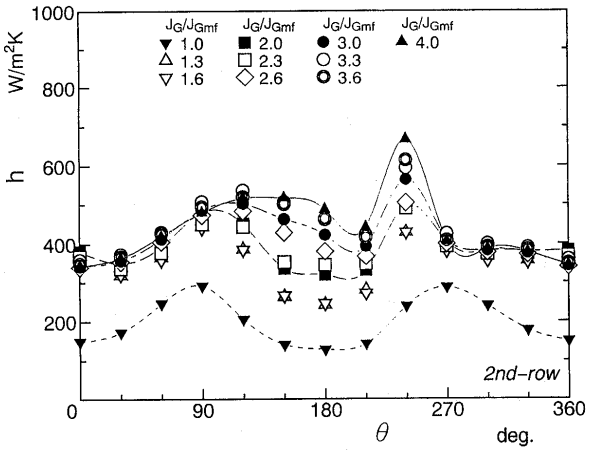

(c) In-line arrangement, $L/D=1.5$, $H/D=1.5$, 2nd row

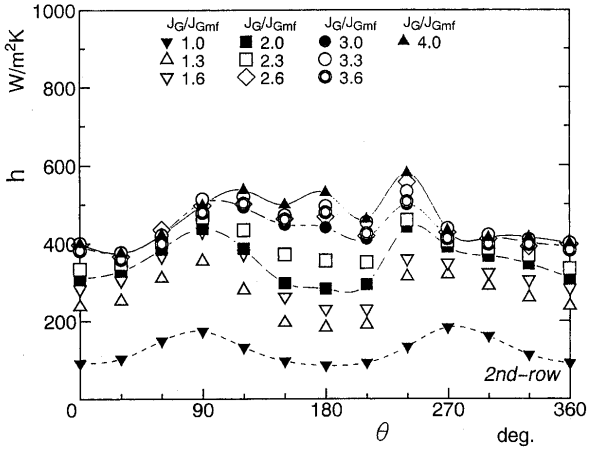

(b) In-line arrangement, $L/D=1.5$, $H/D=2.0$, 2nd row

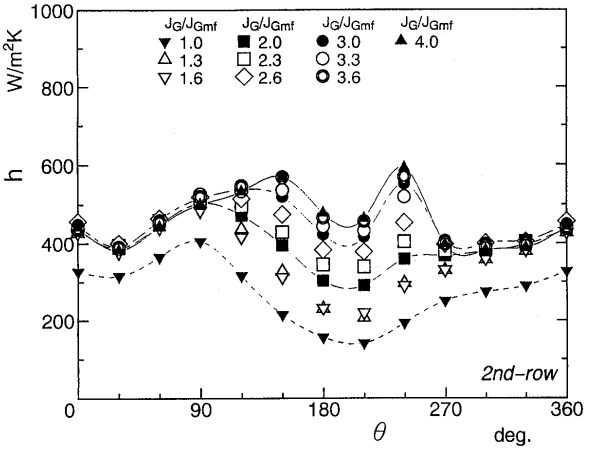

(d) Staggered arrangement, $L/D=1.5$, $H/D=1.5$, 2nd row

Fig. 8 Distribution of heat transfer coefficient around tube

bridging, the heat transfer coefficient for $L/D=1.5$ and $H/D=1.5$, shown in Fig. 8(c), is relatively high compared with that in Fig. 8(b), especially at low gas flux. This difference is interpreted by the difference in flow pattern and the agitation induced. At high gas flux, $J_G/J_{Gmf}=3$ to 4, the heat transfer coefficient shows almost the same distribution around the tube as in the cases of Figs. 8(a) and 8(b).

As regards the staggered arrangement, $L/D=1.5$ and $H/D=1.5$, the heat transfer coefficient shows higher values than those in the in-line arrangements, as shown in Fig. 8(d). The heat transfer coefficient is lower in the wake region than in the upstream stagnation region, especially at low gas flux. This is mainly caused by the jet passing through the side passage of the 1st row and impinging directly on the upstream stagnation region of the 2nd row tube. An increase in the gas flux induces relatively uniform distribution of heat transfer coefficient around tube, similar to the other three cases of Figs. 8(a) to 8(c). As is demonstrated in these figures, the heat transfer coefficient is significantly influenced by the flow pattern in the tube banks.

6. Average Heat Transfer Coefficient

The average heat transfer coefficient h_m around the tube is shown on Nusselt number Nu vs. Reynolds number Re plane in Fig. 9, where Nu and Re are defined by the average particle diameter as the representative length scale and thermo-physical properties of gas, i.e. $Nu=h_m d_p/k_G$ and $Re=d_p J_G/\nu_G$, k_G: thermal conductivity of gas and ν_G: kinematic viscosity of gas. The heat transfer coefficient increases with an increase in the volumetric gas flux. Beyond the Reynolds number $Re=2.2$ (the volumetric flux ratio $J_G/J_{Gmf}=3$), the heat transfer coefficient tends to a constant value. This is interpreted by a balance between two effects, i.e. the deterioration of heat transfer due to high void fraction and the enhanced agitation or convection. Moreover, this tendency

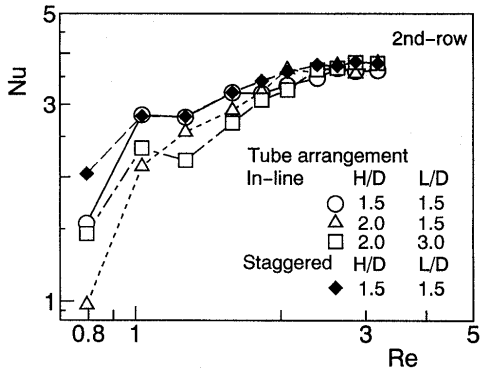

Fig. 9 Average heat transfer coefficient

having constant value at high Reynolds number corresponds to the fact that the void fraction fluctuation has almost the same statistical characteristics at high gas flux condition[8].

The difference in the tube arrangement is typically observed in the heat transfer coefficient at low gas flux condition. An increase in the gas flux and thus the enhanced agitation brings about weak dependence of heat transfer on the tube arrangement. As is discussed in the preceding section, the heat transfer coefficient becomes the highest when the tube arrangement is staggered arrangement and $L/D=1.5$ and $H/D=1.5$. The in-line arrangement with rather small pitch, e.g. $L/D=1/.5$ and $H/D=1.5$, has slightly smaller heat transfer coefficient than that for the staggered arrangement.

7. Conclusion

Neutron radiography was successfully applied to visualize the simulated fluidized-bed with tube banks. The image processing technique gave quantitative distributions as well as fluctuation characteristics of the void fraction. The influence of tube arrangement on the heat transfer characteristics was discussed with reference to the observed flow pattern and void fraction behavior. The next step in this research will be the formulation of heat transfer process on the basis of the presented flow pattern as well as the void fraction fluctuation, which is now on the way. Those who are interested in the visualized image and/or the processed image (in VHS video tape) of fluidized-bed by neutron radiography are welcome to contact e-mail address "ozawa@kansai-u.ac.jp".

Acknowledgment

This investigation was partly supported by the Research Fund, Kansai University (1996). The authors express their sincere thanks to JAERI for making use of the Neutron Radiography System in JRR-3 M. Thanks are extended to Messes. K. Fukuda and J. Nanpei for their support in the experimental work.

References

(1) Horio, M., Combustion and Thermal Engineering, Chapt. 11, The Society of Chem. Engineers, Japan ed., (1987), p. 207-219, Maki Pub, Tokyo.

(2) Saxena, S.C., Grewal, N.S., Gabor, J.D., Zabrodsky, S.S. and Galershtein, D.M., Heat Transfer between a Gas Fluidized Bed and Immersed Tubes, Advances in Heat Transfer, Vol. 14, (1978), p. 149-247, Academic Press, N.Y.

(3) Saxena, S.C., Heat Transfer between Immersed Surface and Gas-Fluidized Beds, Advances in Heat Transfer, Vol. 19, (1989), p. 97-190, Academic Press, N.Y.

(4) Kurosaki, Y., Satoh, I. and Ishize, T., Mechanism of Heat Transfer Enhancement of Gas-Solid Fluidized Bed: Estimation of Direct Contact Heat Exchange from Heat Transfer Surface to Fluidized Particles Using an Optical Visualization Technique, Trans. ASME, J. Heat Transfer, Vol. 117, No. 1 (1995), p. 104-112.

(5) Miyamoto, M., Takahashi, K., Jin, R.J., Katoh, Y. and Kurima, J., Unsteady Heat Transfer and Particle Behavior around a Horizontal Tube Bundle near an Expanded Bed Surface of a Gas Fluidized Bed: Conditional Sampling Statistical Analysis, Int. J. Heat Mass Transf., Vol. 38, No. 17 (1995), p. 3263-3273.

(6) Miyamoto, M., Jin, R.J., Katoh, Y. and Kurima, J., An Experimental Study on Particle Behavior and Heat Transfer Characteristics around Horizontal Tube Bundle in Fluidized Beds, Trans. Jpn. Mech. Eng., (in Japanese), Vol. 62, No. 601 (1996), p. 3431-3438.

(7) Ishigai, S., Akagawa, K., Nakanishi, S., Nishikawa, E., Fujii, T. and Ozawa, M., Steam Power Engineering, Chapt. 3, (1989), p. 117-236, Corona Pub. Co., Tokyo.

(8) Ozawa, M., Umekawa, H., Matsuda, T., Takenaka, N., Tsuruno, A. and Matsubayashi, M., Measurement of Dynamic Behavior of Void Fraction in Tube-Banks of a Simulated Fluidized-Bed by Neutron Radiography, Proc. 5th World Conf. on Neutron Radiography (WCNR), Fischer, C.O., Stade, J. and Bock, W. ed., (1996), p. 610-616, Deutsche Gesellschaft fuer Zerstoerungsfreie Pruefung E. V., Berlin.

(9) Ozawa, M., Umekawa, H., Matsuda, T., Takenaka, N., Tsuruno, A. and Matsubayashi, M., Void Fraction Profile in Tube-Banks of a Simulated Fluidized-Bed Heat Exchanger, Nucl. Instrm. and Methods in Physics Research A, Vol. 377 (1996), p. 144-147.

(10) Ozawa, M., Umekawa, H., Matsuda, T., Takenaka, N., Tsuruno, A. and Matsubayashi, M., Large Particle Movement and Drag Coefficient in a Fluidized Bed, Trans. Jpn. Soc. Mech. Eng., (in Japanese), Vol. 62, No. 601 (1996), p. 3413-3420.

(11) Kunii, D. and Levenspiel, O., Fluidization Engi-

neering, 2nd ed., (1991), p. 216-217, Butterworth-Heinemann, Boston.
(12) Jones, P.J. and Leung, L.S., Fluidization, Davidson, J.F., Clift, R. and Harrison, D. ed., Chapt. 8, (1985), p. 293-329, Academic Press, London.
(13) Ozawa, M., Tobita, S., Mii, T., Tomoyasu, Y., Takebayashi, T. and Suzuki, K., Flow Pattern and Flow Behavior of Solid Particles in L-Valve, Circulating Fluidized Bed Technology III, Basu, P., Horio, M. and Hasatani, M. ed., (1991), p. 615-620, Pergamon Press, Oxford.